BeBeC-2020-D29

DESIGN AND USE OF A THREE-DIMENSIONAL ARRAY OF MEMS MICROPHONES FOR AEROACOUSTIC MEASUREMENTS IN WIND-TUNNELS

Yinshi Zhou[1], François Ollivier[2], Pascal Challande[2], Régis Marchiano[2], Vincent Valeau[1]
David Marx[1], Christian Prax[1]
[1]Institut PPRIME UPR 3346, CNRS-Université de Poitiers-ENSMA
B17-6, rue Marcel Doré, 86022 Poitiers, France
[2]Sorbonne Université, CNRS, Institut Jean Le Rond d'Alembert
4 Place Jussieu, 75005 Paris, France

Abstract

This paper introduces a three-dimensional (3D) microphone array associated with a dedicated beamforming algorithm for aeroacoustic sources identification in an anechoic wind-tunnel. The array is arranged into a "tunnel geometry" composed of three nearly perpendicular planar sub-arrays consisting of 768 digital Micro ElectroMechanical Systems (MEMS) microphones enclosing the $\frac{3}{4}$ open test-section of the wind-tunnel. This setup enables to scan a volume containing the potential noise sources in the wind-tunnel flow. Digital MEMS microphones allow significant cost reduction and lower complexity for large array systems. Several spatial arrangements of the microphones were investigated in terms of resolution and signal-to-noise ratio using synthetic noise sources in order to find the optimal one under manufacturing constraints. The coordinates of the microphones after installation of the array system were obtained by using a method based on the differential times of arrival. The array processing algorithm is based on a 3D implementation of the beamforming technique, associated to the Clean-SC method extended to applications involving dipolar sources, in order to improve the spatial resolution of the 3D sound maps. The application results presented in this study concern the dipolar broadband noise sources radiated by two wall-mounted NACA 0012 airfoils.

1 INTRODUCTION

Microphone arrays are nowadays very common tools in wind-tunnels for performing experimental aeroacoustics studies. Most of the time, planar arrays are used. Such arrays are powerful

tools to identify the sources of sound in a plane parallel to the array, but their resolution is bad perpendicularly to the array so that they fail to perform source identification in three dimensions. However, this aspect is important for studying the sound radiation of obstacles which are strongly three-dimensional (3D). Such studies can be achieved only by using 3D arrays, measuring the sound radiation over a large solid angle around the source, in order to capture the 3D patterns of the radiation.

In 2010, Dougherty [4] reported the design of a cylindrical cage array of 105 pressure transducers enclosing a jet. Diverse beamforming techniques were evaluated to investigate the noise sources at low frequency. Padois *et al.* [12] used four sub-arrays of 48 microphones mounted on the walls of the closed test-section of a wind-tunnel, and applied their system to the aelioan tones produced by a cylinder. Porteous et al. [13] used two perpendicular arrays of 31 microphones to investigate the radiation of cylinders and airfoils; the originality of their study was the use of a 3D beamforming algorithm (associated to the CLEAN-SC deconvolution technique [15]) taking into account the dipolar nature of the radiation. In 2017, Ernst *et al.* [5] designed a 3D array by optimizing the microphone positions in order to reduce the side lobes in three-dimensional space. In the present study, some measurements are carried out in a wind-tunnel with an open test-section. A large array has been designed, with a tunnel shape totally enclosing the test-section. Such an array requires a high number of microphones (of the order of several hundreds), in order to reach a targeted operational frequency range reaching frequencies of the order of 10 kHz.

Large microphone arrays are still rare nowadays because the technological barriers remain numerous: the congestion of the connections, the complexity of the electronic design and manufacturing of the system, maintenance complexity to replace faulty channels, the difficulty and time required to deploy the system *in situ*. To defeat these locks, a strategy is to propose an architecture dividing the array into sub-arrays. The advantage lies in the ability to position subsets over a large area, and in the fact that it requires a number of wires lower than the number of microphones. Silverman *et al.* were pioneers in making large arrays in the late 1990s, with the Huge Microphone Array, made up of 512 electret microphones [16]. The architecture was broken down into 16-microphone modules containing the analog-to-digital conversion and then connected by optical fiber to the master interface. The LOUD array, designed at MIT in 2004, has long been the largest network, equipped with 1020 channels [20]. In this purpose, the team designed the most modular structure possible: the instrumentation chain is compacted closer to each microphone. This has two important advantages: (i) ease of manufacture and maintenance: all modules are identical, and can easily be replaced in the event of a failure, (ii) the signal transmission is entirely digital. But this array of transducers was still very complex and its shape was only two-dimensional. In 2004, Humphreys *et al.* [7] designed a planar array of 128 analog microphones which solved the problem of complexity of the conditioning stage. The application to a scaled landing gear indicated performances equivalent to arrays of measurement microphones.

In this study, we propose to use a massive multi-channels antenna in order to build a 3D array: the MegaMicros system, developed at Institut d'Alembert [18]. This new generation of array is based on the use of a large number of digital MEMS (Micro ElectroMechanical Systems) microphones (up to 1024). This 3D array will be used in this paper to investigate the noise produced by two wall-mounted NACA 0012 airfoils.

The present paper is structured as follows. In Section 2, the data acquisition system is first

briefly presented. In Section 3, the experimental set-up (wind-tunnel, test cases) and the characteristics of the 3D array (response of the microphones, design and optimization of the array geometry) are presented. The array processing techniques used, based on 3D beamforming, are introduced in Section 4, followed by results concerning the two wall-mounted airfoils located in the wind-tunnel test section . The paper ends with a set of conclusions (Section 5).

2 ACOUSTIC DATA ACQUISITION SYSTEM

The acoustic data acquisition system allows to synchronously acquire up to 1024 digital signals from MEMS microphones and 16 other signals from analog channels. The 1024 MEMS microphones are divided into 128 bundles of 8 microphones. Each microphone is inserted in a small PCB card (see Fig. 1). In each bundle, the 8 microphones are controlled by a buffer card (see Fig. 1) linked to the data acquisition system with a RJ45 cable (see Fig. 2). First, the data acquisition system collects all the signals acquired by each channel (digital and analog ones). The MEMS microphones are ICS-43434 microphones developed by InvenSense. These microphones deliver digital signals: the whole instrumentation chain is directly included on the chip (the transducer, an amplifier and a 24 bits AD converter). From the microphone to the interface, signals are handled with I2S serial protocol. The sampling frequency can be chosen by the user up to 50 kHz. Then, the 24-bit integer samples are converted to 32-bit floats before multiplexing and transfer via the USB 3.0 serial bus to the host PC.

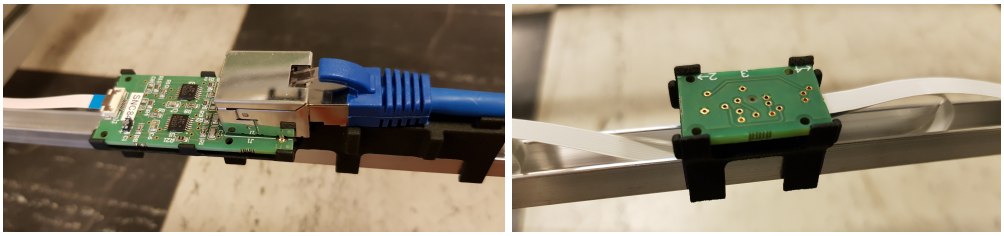

Figure 1: Photograph of a buffer card and of a microphone card.

Figure 2: Photograph of the acoustic data acquisition system. The colored cables are RJ45 linking the buffer cards to acquisition system.

3 EXPERIMENTAL SET-UP

3.1 Wind-tunnel and test models

Wind tunnel The anechoic wind-tunnel BETI of the PPRIME Institute is an open circuit wind-tunnel for aerodynamic and aeroacoustic studies. The wind-tunnel flow is drawn by fan assemblies downstream the test section with suction. Figure 3 shows the sketch of a part of the wind-tunnel. The open test section with a wood plank as bottom is located in an anechoic room of 90 m^3 allowing a cutoff frequency of 200 Hz. The length of the test section in wind-tunnel flow direction is 1.44 m. The wind-tunnel flow is firstly accelerated in a tunnel with decreasing section area (with a contraction ratio of 10), and enters the test section from a rectangular nozzle of (0.7×0.7) m^2. At the nozzle exit, the boundary layer thickness is of the order of 10 mm, and the turbulence intensity of the free-stream flow is about 1.5 %. The flow is then sucked through a collector of dimensions (width $\times$ height) (1.00×0.87) m^2. The maximum free-stream velocity of the wind-tunnel flow is up to 60 m/s (216 km/h). The coordinate system (O,x,y,z) used for the experiments in this paper is presented in Fig. 3. The origin of the coordinate system is located at the center of line AB (see Fig. 3). Axis x follows the wind-tunnel flow direction, and axis z follows the vertical direction.

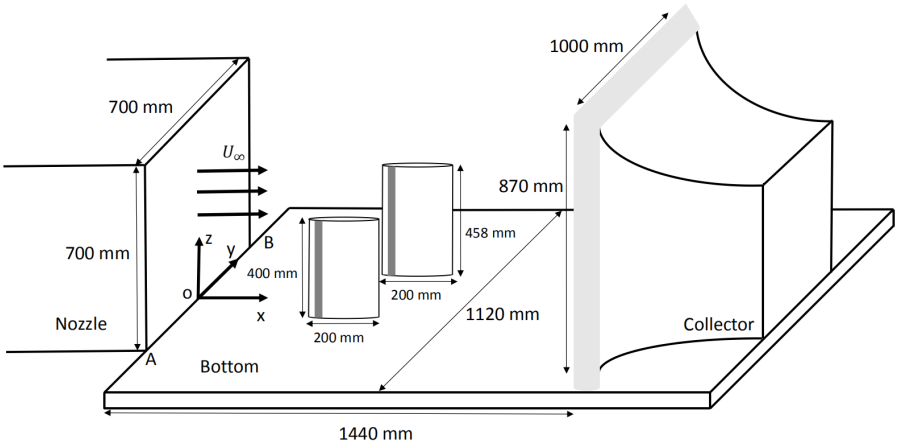

Figure 3: Sketch of the test section of the anechoic wind-tunnel of the PPRIME Institute.

Test models The test models under study are two wall-mounted finite length NACA 0012 airfoils with a flat-ended tip and sharp trailing edge. They both have a chord length $C = 200$ mm. The short NACA 0012 airfoil has a span length $L_1 = 400$ mm and its leading edge is located 350 mm downstream of the nozzle exit at zero-angle of attack. The long NACA 0012 airfoil has a span length $L_2 = 458$ mm and its leading edge is located 450 mm downstream of the nozzle exit at zero-angle of attack. The airfoil models are mounted vertically to the bottom of the open test section as shown in Fig. 4. The distance between them in the y direction is 200 mm. For the two wall-mounted airfoils, a tripping device using a rough band (sandpaper) with a width of 15 mm is placed at a distance of 10 mm from the leading edge along the span at one side of the airfoil surface. Hence, a forced transition of boundary layer can occur on the side with such devices and a natural transition of boundary layer can occur on the other side of the

airfoil surface. The rotation axis of the NACA airfoils are located at 66.6 mm (a third of the chord length) from the leading edge. The angle of attack is defined as positive when the tripping device is on the pressure side of the airfoil. In this paper, results are given for angle of attack at 4° and a flow speed of 50 m/s, corresponding to a chord-based Reynolds number of 6.66×10^5. Tonal noise generation is eliminated at these testing conditions, and it is the broadband noise that dominates the noise radiation.

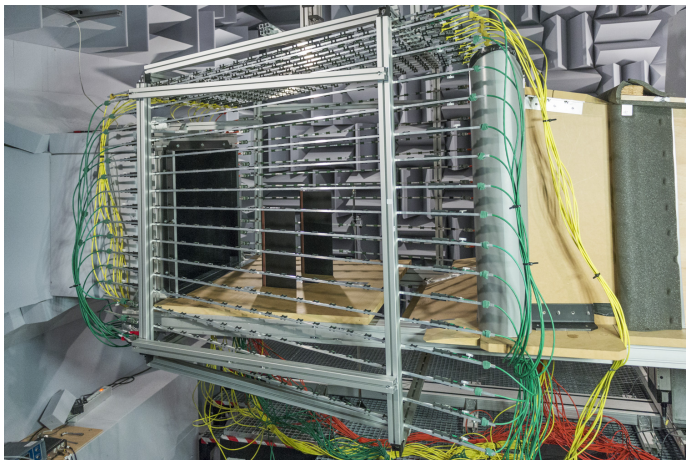

Figure 4: Photograph of the experimental setup. The tunnel-shaped 3D array encloses the nozzle, the two wall-mounted airfoils and the collector from the left to the right in the picture.

3.2 Response of the MEMS microphones

In order to characterize the frequency response the MEMS microphones, 32 elements of a same lot of ICS-43434 have been tested in an anechoic room, using the protocol described in [19].The average response of this set is presented on Fig. 5, together with the intervals of variation in relative amplitude and phase.

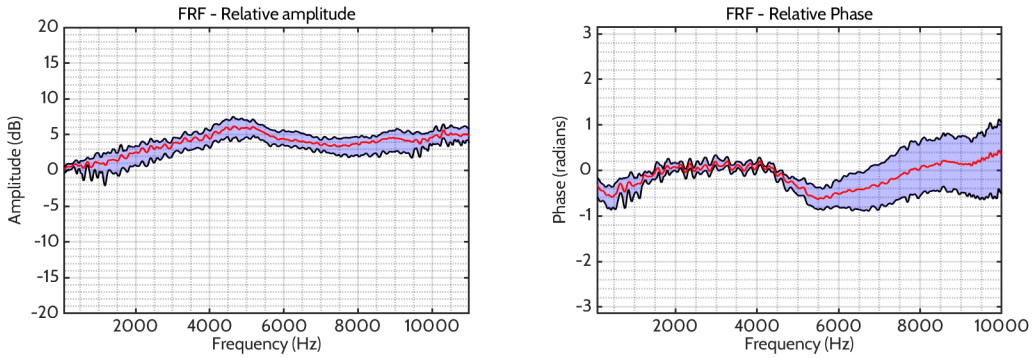

Figure 5: Measured frequency response of a set of 32 MEMS microphones - The measurement protocol follows the procedure depicted in [19]. Red line - Average ; Blue shaded area : variation interval over the set.

The tested set shows a very good homogeneity in terms of sensitivity with less than 3 dB dispersion over the band comprised between 80 Hz and 10 kHz. Concerning the phase homogeneity, it should be noticed that it is very good up to 6kHz. At higher frequencies the relative phase between the microphones grows significantly which is likely to affect the performance of the beamforming process.

Another important point needed to be addressed is the exposure of the microphones to the wind stream. When embedded in a moderate wind, the microphones without any protection are exposed to turbulence and produce saturated signals, hence unusable. Therefore it was required to design the array so as to locate the microphones outside the locus of turbulence. Meanwhile, their distribution was to allow a surrounding view of the aeroacoustic sources while ensuring the best possible characteristics in terms of dynamics and resolution.

3.3 Array design

The minimum distance to the shear layer, the need to avoid the turbulent regions around the collector intake and manufacturing constraints determined a conical shape of array enlarging from the nozzle to the collector intake of the wind tunnel. The structure of the array is shown in Fig. 6. It is a cone with rectangular base surrounding the flow like a tunnel (see also Fig. 4). The length of the edges of square 1 (vertices 1, 2, 3 and 4) is L_1=1200 mm and that of square 2 (vertices 5, 6, 7 and 8) is L_2=1535 mm. The distance between the two squares is L_D=1157 mm. For each of the four sides (A, B, C and D), there are 16 bars (spaced by a distance of 75 mm on square 1 and 96 mm on square 2) . The bars of length 1.8 m have U-shaped section. On each bar there are two bundles of microphones (so 16 microphones on each bar) uniformly spaced by a distance of 72 mm. Each bundle is connected to the acquisition system with an RJ45 cable. The theoretical performances of such an arrangement of the microphones are discussed in the next section. The experiments in this paper were conducted using only 3 sides (A, B and C) enclosing the $\frac{3}{4}$ open test section of the wind tunnel with 768 microphones.

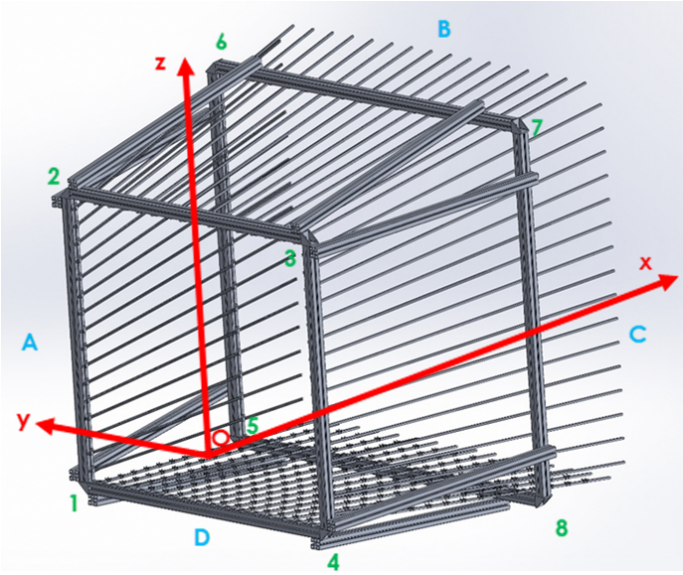

Figure 6: 3D model of the array structure.

3.4 Optimization of the microphones distribution

On the inner surface of the cone surrounding the wind-tunnel flow, various distributions of the microphones could be chosen accounting for the manufacturing constraints and optimal array processing characteristics. Therefore, numerical simulations were conducted to estimate the point spread functions of the possible distributions. Four distributions where compared: fully random (*"Aleat"*), stream-wise logarithmic (*"Log16"*), regular 1 (*"Reg16"*) and regular 2 (*"Reg24"*). They are presented in Fig. 7. To estimate their performances, a harmonic point source is simulated at the center of the volume for investigation. It emits a harmonic signal at a chosen frequency. The signals received at the microphones are polluted by a level driven random noise. Using these signals, a standard beamforming is processed to recover the source. Figure 8 presents a typical result showing the reconstructed acoustic intensity in 3 perpendicular planes intersecting at the source point. The Point Spread Function (PSF) presents two line plots indicating, with respect to the distance to the source over the solid angle 4π, the average relative acoustic level (blue line) and the maximum relative acoustic level (red line).

The investigation established firstly that the random and logarithmic distributions did not provide a significant improvement in terms of dynamics of reconstruction compared to the regular distributions. Therefore, for ease of assembly, the choice was the most regular distribution (Reg16, ie., 16 microphones with a regular longitudinal spacing, on 64 bars with a regular transverse spacing). At high frequency (5kHz) and high noise level (0dB SNR) as shown by Fig. 8, the antenna provides a resolution of a few centimeters with very good dynamic of the order of 10dB in the vicinity of the source up to 15dB at 0.5m and more.

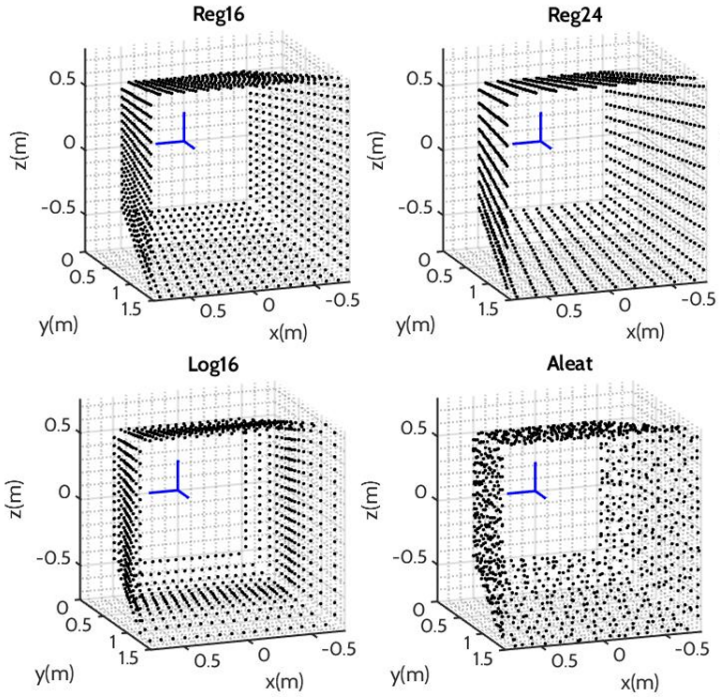

Figure 7: 4 Microphones distribution configurations for the numerical simulation of the PSF.

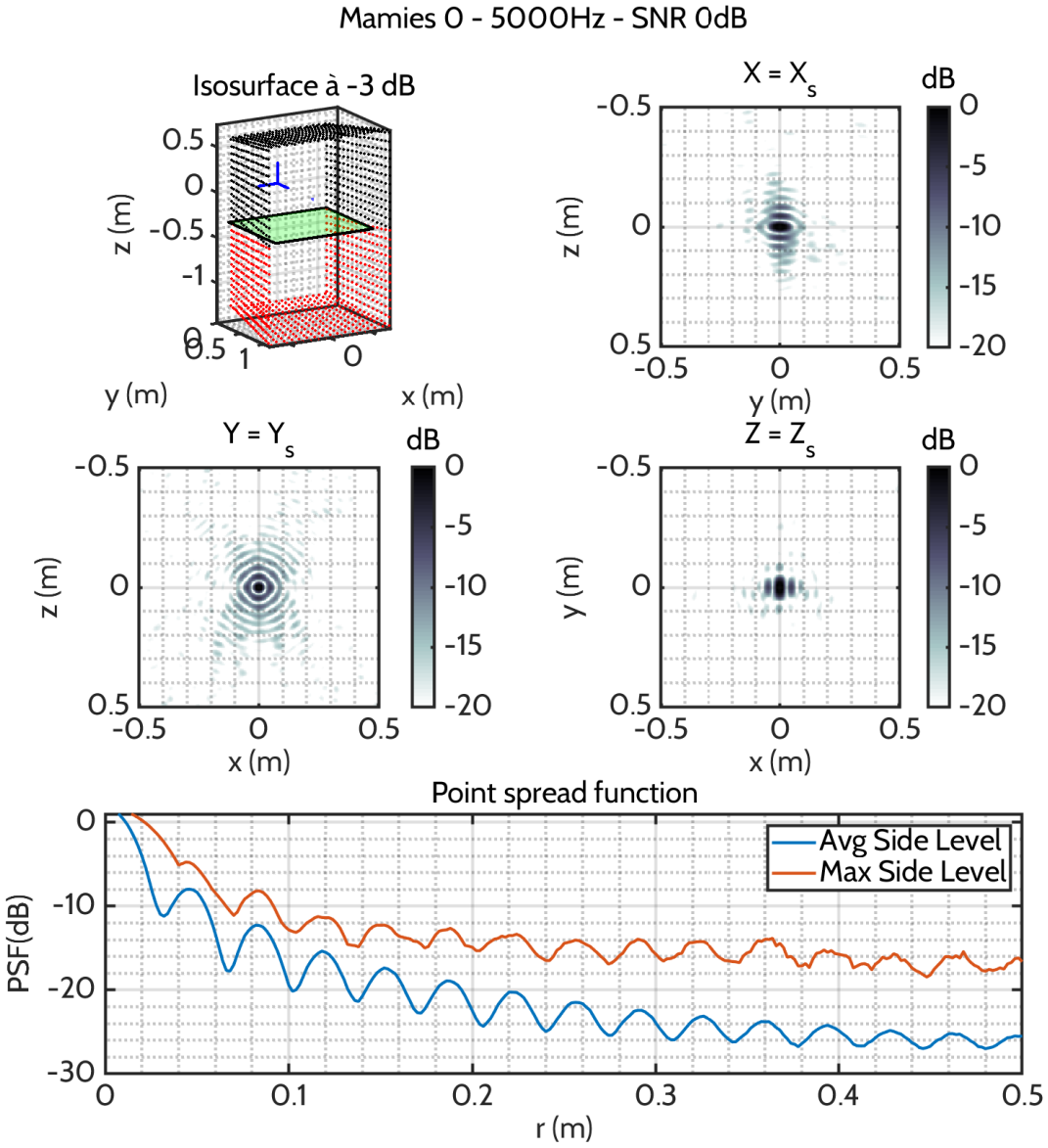

Figure 8: Simulated characteristics of the final array with three panels and 768 microphones. The test case concerns a monopole point source located at the center point of the investigated volume. The signal is harmonic with a frequency of 5 kHz. A random noise is added to the microphone signals with a 0 dB SNR. The floor is considered as a perfectly reflective plane.

3.5 Geometrical calibration of the array

In order to ensure a proper resolution of the inverse problem, the true positions of the microphones have to be assessed. Since the array structure is rigid, this assessment is not critical, the relative positions being well known. Anyway, for a final check of the setup, a thorough geometrical calibration procedure was led. Based on the measurements of relative time of flights between a number of sources and the microphones, it followed the prescriptions of Vanwynsberghe et *al.*[17] to estimate the individual positions of the microphones.

A small loudspeaker was located successively at 29 different positions of the space surrounding the array (12 outside, 17 inside), emitting at each position a broadband signal allowing to implement in the following a generalized cross correlation based process to derive the required set of DTOAs (Differential Time of Arrival). The robust DTOA procedure finally provided a geometry very close to the one measured during the building process, and the latter was used in the array signal process to identify the aeroacoustic sources.

4 ARRAY PROCESSING TECHNIQUE AND RESULTS

4.1 Array processing technique

3D beamforming Conventional beamforming is the standard array processing technique for noise source identification [8, 11]. Consider an array consisting of M microphones located in the far-field of noise sources for identification with $\boldsymbol{x_m}$ describing their position. A scanning domain, which is discretized and represented by a scanning grid (described by the position $\boldsymbol{x_f}$), contains the potential noise sources. It is a plane, generally parallel to a planar array for 2D beamforming and a volume for 3D beamforming.

For each point $\boldsymbol{x_f}$, the frequency-domain beamforming function is given by the following equation:

$$A(\boldsymbol{x_f},\omega) = \frac{\boldsymbol{e}^H \boldsymbol{C_t} \boldsymbol{e}}{M^2 - M}, \tag{1}$$

where $\boldsymbol{C_t}$ is obtained by setting the diagonal elements of the Cross Spectral Matrix (CSM) as zero. The CSM is defined as $\boldsymbol{C} = \boldsymbol{P}\boldsymbol{P}^H$ with ^{H} being the Hermitian transpose operator. This matrix $\boldsymbol{C}$ has an Hermitian symmetry ($C_{mn}(\omega) = C^*_{nm}(\omega)$). $\boldsymbol{P} = (P(\boldsymbol{x_1},\omega)...P(\boldsymbol{x_M},\omega))^T$ contains the Fourier transforms of the signals recorded by each microphone with ^{T} indicating the transpose operator. The steering vector $\boldsymbol{e} = (e(\boldsymbol{x_1},\boldsymbol{x_f},\omega)...e(\boldsymbol{x_M},\boldsymbol{x_f},\omega))^T$ allows the microphone array to "steer" to different scanning points $\boldsymbol{x_f}$, and depends on a source model. Sound maps can be obtained by mapping the beamformed values $A(\boldsymbol{x_f},\omega)$ to the corresponding scanning domain.

For 3D beamforming, the assumption of monopole noise source with uniform radiation is not always appropriate. The flow-induced noise with the presence of solid boundaries tends to have a dipolar radiation [6]. According to [10, 13], the steering function for a point dipole source is given by:

$$e_d(\boldsymbol{x_m},\boldsymbol{x_f},\omega) = exp(-j\omega\tau(\boldsymbol{x_m},\boldsymbol{x_f}))\left(\boldsymbol{\xi}\cdot\frac{\boldsymbol{x_m}-\boldsymbol{x_f}}{r_m}\right), \tag{2}$$

with $r_m = |\boldsymbol{x_m}-\boldsymbol{x_f}|$, c_0 being the speed of sound and $\boldsymbol{\xi}$ being the orientation of the dipole source. The time delay $\tau(\boldsymbol{x_m},\boldsymbol{x_f})$ is simply r_m/c_0 for a quiescent medium. The steering vector allows

to exhibit a main lobe at the position of a dipolar source on sound maps. However, appropriate assumption of the dipole orientation should be made, otherwise it may lead to ambiguous lobes on sound maps.

The wind-tunnel flow can involve significant effects (refraction, convection) on sound propagation, and methods based on ray tracing [1, 9, 14] can be used to compute the time delay $\tau(\boldsymbol{x_m}, \boldsymbol{x_f})$. Note that noise sources on sound maps are subjected to apparent shift downstream if these influences are not considered. In this paper, a 3D implementation of the Amiet's method [2] was used for the beamforming technique. The shear layers of the wind-tunnel were simplified to two vertical planes and a horizontal plane with no thickness. The acoustic rays in the wind-tunnel are not straight from source to microphone because of the convection effect by the wind-tunnel flow and refraction effect by the shear layer. In this paper, only the angle corrections due to the shear layers of the wind-tunnel are addressed, and the existence of the wake of the airfoils is not accounted for in the Amiet's method.

Deconvolution The main lobes of the beamforming sound maps are used to identify the location of noise sources. However, they provide the source location and its distribution only approximately because the size of the lobes are frequency-dependent. Moreover, side lobes may contaminate the beamforming results because they can overlap between them and even with main lobes. This makes it difficult to obtain the real distribution of noise source. To improve the spatial resolution in all frequency bands and remove the side lobes from the sound maps, the deconvolution method CLEAN-SC (Sijtsma [15]) can be associated to the BF technique. This method is not computationally expensive and can be extended to 3D applications for dipolar noise sources, which was initially developed by Porteous *et al.* [13]. Although it is not efficient at low frequencies and for source regions containing coherent noise (Bahr and Cattafesta [3]), it is used in this paper based on its good compromise between efficiency and computational cost.

4.2 Results

Acoustic measurements were conducted with the 768 digital MEMS microphones and a microphone (GRAS 40F) placed outside the flow above the airfoil surface at the level of the trailing edge of the longer airfoil. The experiment data were transmitted using 769 channels including an analogical channel for the GRAS microphone. They were obtained for a sampling time of 5 s with a sampling frequency of 50 kHz. The analogical data were used to compute the far-field spectrum of the two wall-mounted airfoils in flow. For the acoustic spectrum and sound maps, the Welch's method of spectral estimation was used, and the frequency resolution was 20 Hz.

In order to compute the sound maps, 236 channels of acoustic data were selected from the acoustic database containing 768 channels. The scanning domain is a cube of dimension 0.6 m $\times$ 0.6 m $\times$ 0.6 m containing a 3D scanning grid of 226981 points (61^3) (see Fig. 9), for which the grid was composed of cubes with an edge length of 10 mm. As explained above, a dipolar noise source model was used for beamforming processing. Therefore, the steering vectors were computed based on Eq. (2), with the dipole orientation perpendicular to the airfoils' surfaces. The 3D sound maps were presented in a third-octave band [2828 Hz; 3564Hz] of centre frequency 3175 Hz, which were obtained by summing all the beamforming results in this band.

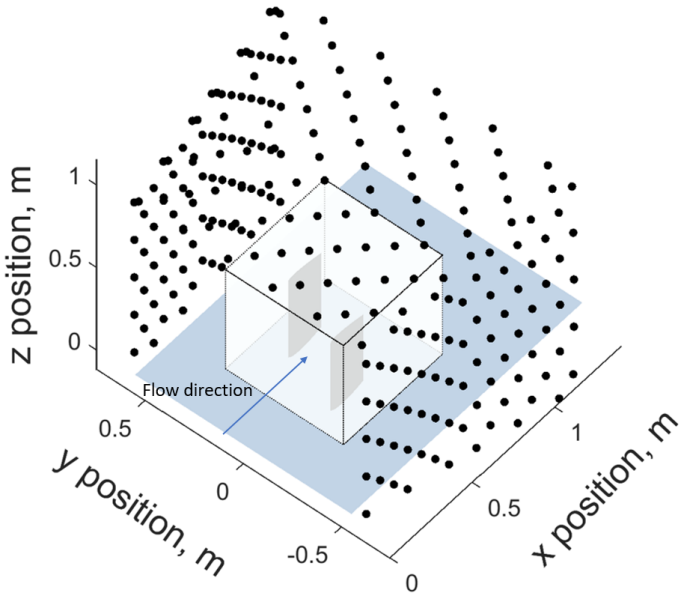

Figure 9: Schematic depicting the positions of microphones of the 3D array with black points and the two wall-mounted airfoils. The cube with dashed edges of dimension 0.6 m $\times$ 0.6 m $\times$ 0.6 m presents the 3D scanning grid for the beamforming. The blue plane indicates the bottom of the open test section of the wind tunnel.

Fig. 10 shows the wideband far-field spectrum of the noise generated by the two wall-mounted airfoils at angle of attack $\alpha = 4°$ and incoming velocity $U_\infty = 50$ m/s. The acoustic spectrum in the band [2828 Hz; 3564Hz] is the part between the blue lines (see Fig. 10).

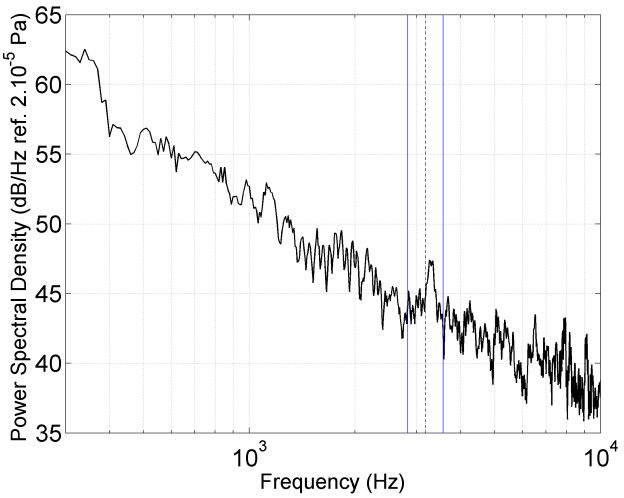

Figure 10: Far-field acoustic power spectral density (dB/Hz ref. 2.10^{-5} Pa) for the two wall-mounted finite airfoils at angle of attack $\alpha = 4°$ and incoming velocity $U_\infty = 50$ m/s. The two blue lines present the third-octave band [2828.4 Hz; 3563.6Hz]. The dash-dot line presents its center frequency 3174.8 Hz.

Fig. 11 shows the sound maps of the two wall-mounted airfoils in the third-octave band [2828 Hz; 3564Hz] at angle of attack of $\alpha = 4°$ and incoming velocity $U_\infty = 50$ m/s. In Fig. 11(a), the beamforming result illustrates some lobes around the trailing edges of the two wall-mounted airfoils. A lobe with large size along the trailing edges may indicate some noise sources. However, regular appearance of some lobes of almost the same size in the direction perpendicular the airfoils' surfaces is observed, which introduces the ambiguity for the distribution of the noise sources. In Fig. 11(b), the CLEAN-SC technique allows a better spatial resolution for the sound map. The safety factor and clean beamwidth for CLEAN-SC were set respectively as 0.99 and 5 cm. After removing the side lobes, the distribution of the broadband noise generated by the airfoils is clearly observed. For the longer airfoil, the noise source distributes evenly along the trailing edge of the airfoil with higher sound intensity toward the wing tip area. For the airfoil with short span, this tendency is stronger with the wing tip noise dominating the noise generation of this airfoil. It is suggested that the wing tip flow has more influence on the flow mechanism in the mid-span area at the trailing edge of the short airfoil and thus on the corresponding noise source distribution.

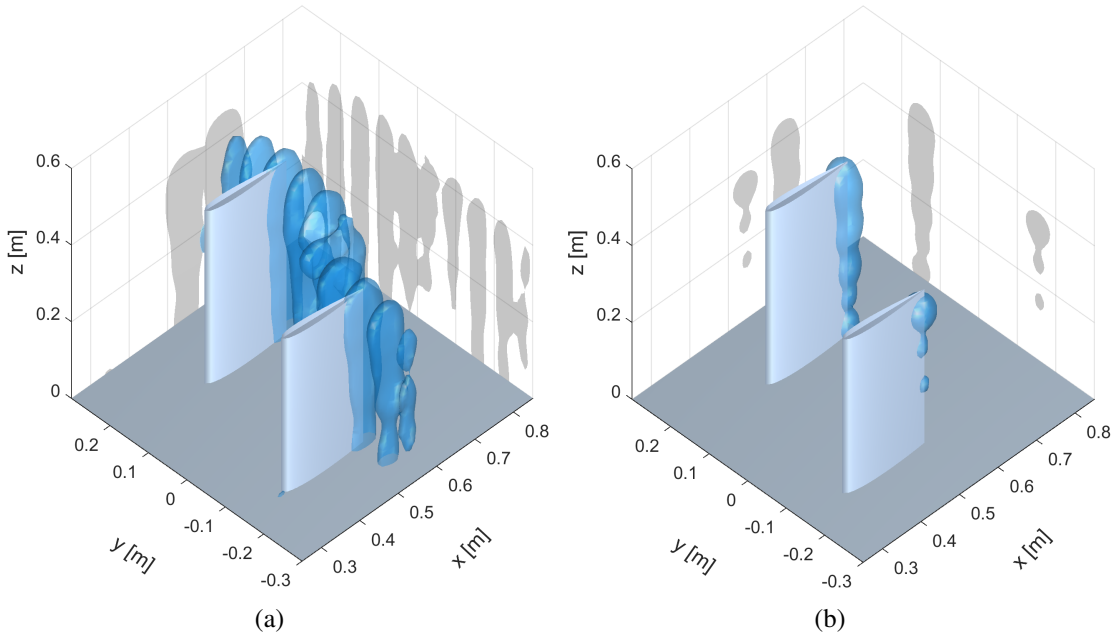

Figure 11: Sound maps for the wall-mounted finite airfoils at incoming velocity $U_\infty = 50$ m/s and angle of attack $\alpha = 4°$, at a third-octave band [2828 Hz; 3564Hz] of centre frequency 3175 Hz (a): 3D dipolar beamforming; (b): CLEAN-SC technique. The 3D isosurface in each sound map is plotted at 6 dB below the maximum. The shadows present the 3D beamforming results projected in different directions.

5 CONCLUSIONS

This paper introduces the design of a 3D microphone array and its first application to aeroacoustic source identification in an anechoic wind-tunnel. Digital MEMS microphones and the

designed data acquisition system through USB connection allow a large amount of data channels for the 3D array. A 3D array was installed in the wind-tunnel, made of three planar arrays enclosing the open test section. The coordinates of the microphones were estimated, based on the measurements of relative time of flights between a number of sources and microphones. The arrangement of the microphones was chosen in order to optimize the resolution and dynamics of the array, by using simulations,

The array system was applied to the broadband aeroacoustic radiation of two wall-mounted finite NACA 0012 airfoils of different span lengths. An acoustic database containing 769 channels of data (768 MEMS channels and an analogical channel) was obtained. 236 channels of data were selected from the database for array signal processing. A 3D conventional beamforming algorithm with a dipolar noise source model was used, associated to the deconvolution method CLEAN-SC. The flow effects on sound propagation were taken into account by using the Amiet's method. The broadband noise sources generated by the two airfoils were successfully identified on the 3D sound maps, in terms of distribution, in a third-octave band.

ACKNOWLEDGEMENTS

The authors warmly acknowledge Jacques Marchal, Hugo Dutilleul, Hélène Moingeon, Christian Ollivon (Institut d'Alembert), and Pascal Biais, Janick Laumonier, Laurent Philippon, Philippe Szeger, Jean-Christophe Vergez (Institut PPRIME) for their invaluable technical support. This work is supported by Agence Nationale de la Recherche (ANR) and China Scholarship Council.

References

[1] R. Amiet. "Refraction of sound by a shear layer." *J. Sound Vib.*, 58(4), 467–482, 1978.

[2] C. Bahr, N. S. Zawodny, T. Yardibi, F. Liu, D. Wetzel, B. Bertolucci, and L. Cattafesta. "Shear layer time-delay correction using a non-intrusive acoustic point source." *International Journal of Aeroacoustics*, 10(5-6), 497–530, 2011.

[3] C. J. Bahr and L. N. Cattafesta. "Wavenumber–frequency deconvolution of aeroacoustic microphone phased array data of arbitrary coherence." *J. Sound Vib.*, 382, 13–42, 2016.

[4] R. Dougherty. "Jet noise beamforming with several techniques." In *Berlin Beamforming Conference (Berlin, Germany)*. 2010.

[5] D. Ernst and C. Spehr. "A three-dimensional microphone array for wind tunnel application." In *Internoise 2017 (Honk-Kong)*. 2017.

[6] M. Howe. "The influence of solid boundaries upon aerodynamic sound." *Proc. Royal Soc. of London. Series A, Mathematical and Physical Sciences*, 231(1-2), 505–514, 1955.

[7] W. Humphreys, Q. Shams, S. Graves, B. Sealey, S. Bartram, and T. Comeaux. "Application of MEMS microphone array technology to airframe noise measurements." In *11th AIAA/CEAS Aeroacoustics Conference (Monterey, California)*, page 3004. 2005.

[8] D. H. Johnson and D. E. Dudgeon. *Array signal processing: concepts and techniques*. Prentice Hall, Upper Saddle River, USA, 1993.

[9] L. Koop, K. Ehrenfried, and S. Kroeber. "Investigation of the systematic phase mismatch in microphone-array analysis." In *11th AIAA/CEAS Aeroacoustics Conference, Monterey, USA*. 2005.

[10] Y. Liu, A. R. Quayle, A. P. Dowling, and P. Sijtsma. "Beamforming correction for dipole measurement using two-dimensional microphone arrays." *J. Acoust. Soc. Am.*, 124(1), 182–191, 2008.

[11] T. J. E. Mueller. *Aeroacoustic measurements*. Springer, New York, USA, 2002.

[12] T. Padois, O. Robin, and A. Berry. "3D source localization in a closed wind-tunnel using microphone arrays." In *19th AIAA/CEAS Aeroacoustics Conference (Berlin, Germany)*, page 2213. 2013.

[13] R. Porteous, Z. Prime, C. J. Doolan, D. J. Moreau, and V. Valeau. "Three-dimensional beamforming of dipolar aeroacoustic sources." *J. Sound Vib.*, 355, 117–134, 2015.

[14] I. Rakotoarisoa, D. Marx, C. Prax, and V. Valeau. "Array processing for the localisation of noise sources in hot flows." *Mechanical Systems and Signal Processing*, 116, 160–172, 2019.

[15] P. Sijtsma. "CLEAN based on spatial source coherence." *Int. J. Aeroacoustics*, 6(4), 357–374, 2007.

[16] H. F. Silverman, W. R. Patterson, and J. L. Flanagan. "The huge microphone array (HMA)." *J. Acoust. Soc. Am.*, 101(5), 3119–3119, 1997.

[17] C. Vanwynsberghe, P. Challande, J. Marchal, R. Marchiano, and F. Ollivier. "A robust and passive method for geometric calibration of large arrays." *The Journal of the Acoustical Society of America*, 139(3), 1252–1263, 2016.

[18] C. Vanwynsberghe, R. Marchiano, F. Ollivier, P. Challande, H. Moingeon, and J. Marchal. "Design and implementation of a multi-octave-band audio camera for realtime diagnosis." *Applied Acoustics*, 89, 281–287, 2015.

[19] C. Vanwynsberghe, R. Marchiano, F. Ollivier, P. Challande, H. Moingeon, and J. Marchal. "Design and implementation of a multi-octave-band audio camera for realtime diagnosis." *App. Acoust.*, 89, 281–287, 2015.

[20] E. Weinstein, K. Steele, A. Agarwal, and J. Glass. "A 1020-node microphone array and acoustic beamformer." In *International Congress on Sound and Vibration (ICSV)*. 2007.